Chin. Phys. Lett. **39**, 057102 (2022)

Anisotropic Fermi Surfaces, Electrical Transport, and Two-Dimensional Fermi Liquid Behavior in Layered Ternary Boride MoAlB

Pan Nie(聂盼)[1], Huakun Zuo(左华坤)[1], Lingxiao Zhao(赵凌霄)[2*], and Zengwei Zhu(朱增伟)[1*]

[1] *Wuhan National High Magnetic Field Center and School of Physics, Huazhong University of Science and Technology, Wuhan 430074, China*
[2] *Department of Physics, Southern University of Science and Technology, Shenzhen 518055, China*

(Received 2 March 2022; accepted 7 April 2022; published online 29 April 2022)

We report a study of fermiology, electrical anisotropy, and Fermi liquid properties in the layered ternary boride MoAlB, which could be peeled into two-dimensional (2D) metal borides (MBenes). By studying the quantum oscillations in comprehensive methods of magnetization, magnetothermoelectric power, and torque with the first-principle calculations, we reveal three types of bands in this system, including two 2D-like electronic bands and one complex three-dimensional-like hole band. Meanwhile, a large out-of-plane electrical anisotropy ($\rho_{bb}/\rho_{aa} \sim 1100$ and $\rho_{bb}/\rho_{cc} \sim 500$, at 2 K) was observed, which is similar to those of the typical anisotropic semimetals but lower than those of some semiconductors (up to 10^5). After calculating the Kadowaki–Woods ratio (KWR $= A/\gamma^2$), we observed that the ratio of the in-plane $A_{a,c}/\gamma^2$ is closer to the universal trend, whereas the out-of-plane A_b/γ^2 severely deviates from the universality. This demonstrates a 2D Fermi liquid behavior. In addition, MoAlB cannot be unified using the modified KWR formula like other layered systems (Sr_2RuO_4 and $MoOCl_2$). This unique feature necessitates further exploration of the Fermi liquid property of this layered molybdenum compound.

DOI: 10.1088/0256-307X/39/5/057102

Recently, the layered XAB phases ($X =$ transition metal, $A =$ aluminum or zinc, and B is boron) have attracted considerable attention as refractory materials with high melting points, high hardness, and high electrical and thermal conductivities.[1–6] The XAB phase includes several structures ranging from X_2AlB_2 ($X =$ Cr, Fe, or Mn) ($Cmmm$),[7,8] $XAlB$ ($X =$ Mo or W) ($Cmcm$),[9,10] $(CrB_2)_nCrAl$, Cr_3AlB_2 ($Immm$),[4] Cr_4AlB_4 ($Immm$),[4] Ru_2ZnB_2 ($I4_1/amd$),[1,11] and $Ru_3Al_2B_2$.[12] Among them, MoAlB has been intensively studied because of its excellent high-temperature oxidation resistance[1,13,14] and good mechanical properties.[3,12] Kota *et al.* showed that MoAlB exhibits subparabolic oxidation kinetics at temperatures up to 1300 ℃.[13,15] At elevated temperatures, Al deintercalates from the structure to form a dense Al_2O_3 scale that protects the material. The dense bulk demonstrates high oxidation resistance up to 1600 ℃.[12]

Despite structural manipulation difficulties due to thermodynamic stability of refractory materials, deintercalation of Al to obtain two-dimensional (2D) metal borides (MBenes) has been achieved through the chemical exfoliation of the layered compound.[16] The obtained MBenes belong to the MXenes, such as 2D metal carbides and nitrides, which have exhibited applications in supercapacitors, batteries, and 2D hydrogen evolution reaction (HER) catalysts. The basal plane of MoAlB was found to be catalytically active for the HER.[17] The interlayer etching through a reaction with NaOH can increase the surface area and HER activity. Chemical exfoliation provides an accessible approach for obtaining MBenes that may have unique properties compared with their bulk three-dimensional (3D) counterparts.[18]

However, the anisotropic physical properties originating from the layered structure have been less studied. Recently, a colossal 3D electrical anisotropy has been reported. The electrical conductivity was found up to $\rho_{bb}/\rho_{aa} = 1.43 \times 10^5$ for the out-of-plane and $\rho_{cc}/\rho_{aa} = 12.12$ at 2 K. For the in-plane, the conductivity anisotropy is the strongest among the typical in-plane anisotropic materials.[19] The high anisotropy of phonon vibration was verified using angle-resolved polarized Raman spectroscopy.[19] Our previous report revealed a large magnetoresistance (MR) and quantum oscillation (QO) effect in resistivity,[20] indicating a quasi-two-dimensional Fermi surface (FS) structure. The anisotropy of its electronic structure, i.e., the FS, was not thoroughly discussed based on experimental results and theoretical calculations. The relationship between the conductivity anisotropy and the FS were

*Corresponding author. Email: zhaolx@mail.sustech.edu.cn; zengwei.zhu@hust.edu.cn
© 2022 Chinese Physical Society and IOP Publishing Ltd

not elaborated. Additionally, QO frequencies beyond 1100 T were too small to be ascertained.

In addition, little information is available regarding the Fermi liquid property in the transition-metal molybdenum compound with light electron mass. In the Fermi liquid theory, the standard Kadowaki–Woods ratio (KWR)[21] $\alpha = A/\gamma^2$ implies that the transition metals and heavy fermion materials fall on two straight lines with different slopes of $\alpha_{\rm TM} = 0.4\,\mu\Omega{\cdot}{\rm cm}{\cdot}{\rm mol}^2{\cdot}{\rm K}^2{\cdot}{\rm J}^{-2}$ and $\alpha_{\rm HF} = 10\,\mu\Omega{\cdot}{\rm cm}{\cdot}{\rm mol}^2{\cdot}{\rm K}^2{\cdot}{\rm J}^{-2}$, respectively. A is the coefficient of the quadratic increase in low-temperature resistivity, $\rho \sim AT^2$, and γ is the electronic specific heat $C_{\rm el}(T) = \gamma T$.[21,22] A strong correction is one of the reasons for large KWRs in heavy-fermion systems.[23] Several molybdenum compounds have been reported to have strong electron–electron correlation, such as the superconductor Mo_3Sb_7 with the coexistence of spin fluctuation,[24] van der Waals layered material $MoOCl_2$,[25] perovskite molybdates $Ba_{1-x}K_xMoO_3$,[26] and $Sr_{1-x}La_xMoO_3$.[27] Their KWRs are closer to the heavy-fermion line, whereas the KWR slope for the anisotropic transition-metal MoAlB remains unclear.

In this Letter, we present a study involving compensative experiments on QO, electrical anisotropy, and KWR measurements of MoAlB. By measuring the magnetic torque under pulsed magnetic fields of up to 59 T and thermoelectricity, we unambiguously identify more high frequencies, such as one high QO frequency of 2000 T. Using the first-principle calculation, we identify MoAlB's FS, which includes two anisotropic electron bands and one complex hole band. Based on the band structure, we calculated the anisotropic conductivity of MoAlB using the Boltzmann transport theory combined with constant relaxation time approximation with a BoltzTrap code. We found the out-of-plane conductivity anisotropies (∼1100) from the experiment. This anisotropy is larger than those of typical layered metals, such as graphite and Sr_2RuO_4, and smaller than those of semiconductors (MoS_2 and $MoSe_2$) with a typical value of 10^5. Moreover, combining the γ from the zero-field specific heat, we observed that $A_{a,c}/\gamma^2$ lies closer to $\alpha_{\rm TM}$, instead of $\alpha_{\rm HF}$, where most of the other molybdenum compounds lie. However, A_b/γ^2 is much larger and closer to the typical value of heavy fermions.

Experiment and Method. MoAlB single crystals were grown using the flux method.[20] MoAlB single crystals have the typical dimensions of $2 \times 1.7 \times 0.4\,{\rm mm}^3$. The specific heat and transport measurements were performed on a physical property measurement system (Quantum Design PPMS) and TeslatronPT (Oxford Instruments). Electric current was applied through a Keithley 6221 instrument, and voltage was measured using Keithley 2182A. Nernst and Seebeck effects were measured using a standard one-heater-two-thermometers configuration[28] in Oxford instruments. Magnetization was measured in stable field using a magnetic property measurement system (Quantum Design SQUID-VSM) at 7 T, and the torque signal was measured at Wuhan National High Magnetic Field Center using a miniature, commercially available piezoresistive microcantilever. The sample was mounted at the beam end using N grease. The used excitation signal frequency was 131 kHz, which is considerably higher than the cantilever's eigenfrequency.[29] The first-principle density functional theory (DFT) calculations based on the full-potential linearized augmented plane-wave method were performed using the WIEN2k package.[30] $RK_{\rm max}$ was set to 5 because the smallest atom in the compound is boron.[30] A k-point mesh of $21 \times 21 \times 21$ in the first Brillouin zone was used. We utilized the semiclassical electronic Boltzmann transport equation to calculate the anisotropy of conductivity using the BoltzTrap2 code[31] by incorporating it with the DFT results.

Results and Discussion. Figure 1(a) shows the crystal structure of MoAlB. The b axis has the longest lattice constant, up to $b = 14.062$ Å. Figure 1(b) shows the temperature dependence of the resistivity of MoAlB as the electrical current was applied along a, b, and c axes. The in-plane ($I \parallel a, c$) and out-of-plane ($I \parallel b$) resistivities were measured using a standard four-contact setup. The current electrodes was modified into a ring shape to cover maximum area of the crystal surfaces, while the voltage leads were placed at the center of the ring of the current electrodes [the inset in Fig. 1(b)]. The reverse side of the sample with a similar silver paint configuration cannot be shown in the photo. As shown in Fig. 1(c), a high anisotropy of resistivity was observed, which corresponds to $\rho_{bb}/\rho_{aa} \sim 1100$ and $\rho_{bb}/\rho_{cc} \sim 500$ at 2 K, originating from its layered crystal structure. For three scattering contributions through defects, electrons, and phonons in the paramagnetic material, the total electrical resistivity $\rho_{\rm tot}(T)$ dependence of temperature is given by the Matthiessen rule as follows:

$$\rho_{\rm tot} = \rho_0 + AT^2 + BT^5, \tag{1}$$

where ρ_0, AT^2, and BT^5 denote the contributions due to scattering from impurity (e–i), electron (e–e), and phonon (e–ph), respectively.[32] The fitting parameters for both orientations are listed in Table 1. The fitting parameters for the temperature dependence of the in-plane resistivity ($I \parallel a, c$) were obtained from experimental data between 2 and 20 K using formula (1). By contrast, the fitting parameters for the temperature dependence of the out-of-plane resistivity ($I \parallel b$)

were obtained between 13 and 25 K because of a slight up-turn (for more information, please see the discussion presented below) in resistivity below 12 K.

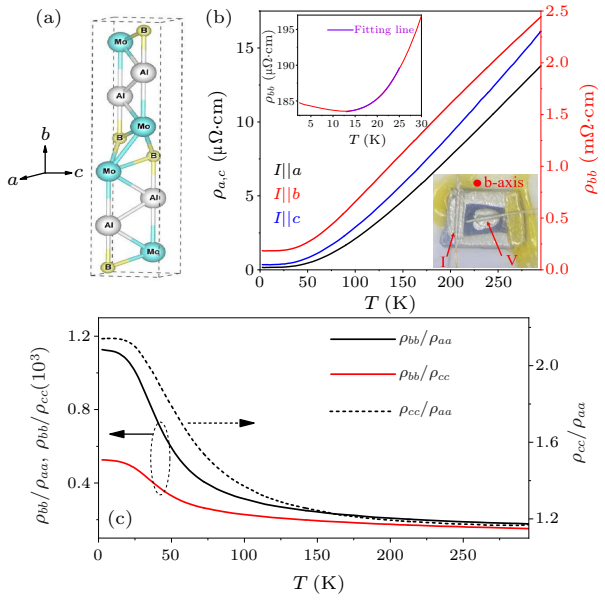

Fig. 1. (a) Crystal structure of MoAlB in the unit cell. (b) Temperature dependence of the resistivity along a, b, and c axes at the zero field. The left inset in (b) is the enlarged temperature range for the experimental result and the fitting line of ρ_{bb}. The right inset shows the four-contact arrangement for measuring ρ_{bb}. (c) Resistivity ratio (ρ_{bb}/ρ_{aa}, ρ_{bb}/ρ_{cc}, and ρ_{cc}/ρ_{aa}) versus temperature.

We explored the QOs using different techniques to precisely map the FS. Although the SdH resolved three frequencies, the amplitudes of the other QO peaks in the FFT spectrum were too weak to be determined.[20] Figure 2(a) shows the magnetization of MoAlB. The magnetization increases linearly with increasing magnetic field up to 7 T. We extracted ΔM as shown in the inset of Fig. 2(a) and the susceptibility $\chi = 9.75 \times 10^{-5}$ emu·Oe^{-1}·mol^{-1} by subtracting the magnetized background signal with a linear fit. Figure 2(b) shows the FFT spectrum of ΔM at 2 K. Three frequencies, i.e., F_α, F_χ, and F_δ, were obtained from the magnetization measurements. Further, we performed thermoelectricity measurements, which are sensitive to QOs at temperatures below 6 K and under magnetic fields up to 14 T. Figures 2(c) and 2(e) present the field dependence of the longitudinal (Seebeck effect S_{xx}) and transverse thermoelectricity (Nernst effect S_{xy}) at different temperatures and reveal more frequencies ($F' = 590$ T and $F'' = 804$ T) than those in the SdH and magnetization measurements, confirming the existence of a high frequency of 2000 T, because of the sensitivity to the QOs of magnetothermoelectric power.

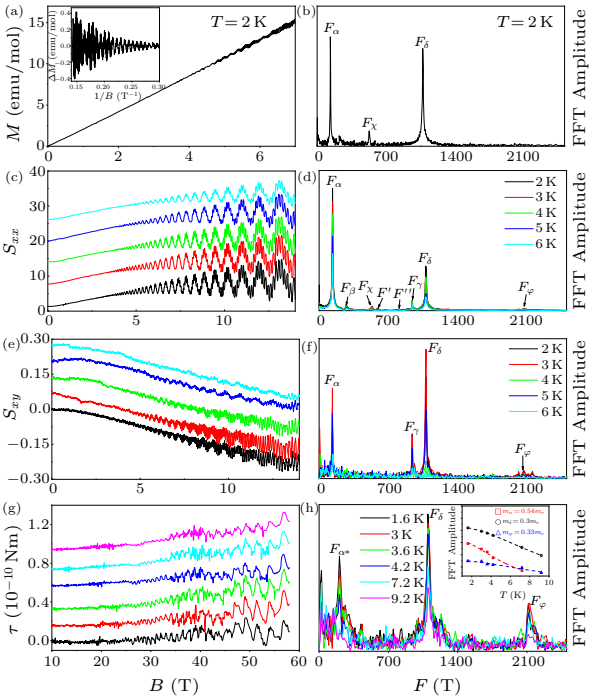

Fig. 2. Quantum oscillations in MoAlB when the field is along the b axis. (a) Magnetization quantum oscillation at 2 K up to 7 T. The inset shows the residual magnetization ΔM after subtracting a linear background as a function of $1/B$. (b) FFT spectrum of ΔM at 2 K. (c) and (e) Seebeck and Nernst effects below 6 K at 14 T. (d) and (f) FFT spectra of S_{xx} and S_{xy} at different temperatures. (g) Field dependence of the magnetic torque τ at various temperatures up to 59 T. (h) FFT spectra of τ at various temperatures. The inset shows the Lifshitz–Kosevich (L-K) fitting with the effective masses.

Table 1. Summary of the quantum oscillation frequency from experimental and theoretical calculations. $F_{\rm MR}$, $F_{\rm M}$, $F_{S_{xy}}$, $F_{S_{xx}}$, and F_τ are obtained via magnetoresistivity, magnetization, Nernst effect, Seebeck effect, and torque, respectively.

Pockets	α	α*	β	β*	χ	F'	F''	γ	δ	η	φ
$F_{\rm MR}$ (T)[20]	134.4		229.5		529			946.2	1080.5	1446(10°)	2060
$F_{\rm M}$ (T)	134				527				1067		
$F_{S_{xy}}$ (T)	134							941	1081		2066
$F_{S_{xx}}$ (T)	135			275	532	590	804	940	1080		2067
F_τ (T)		205							1100		2114
Pocket-$E1$ (calculated) (T)	137	193	250	307		559					
Pocket-$E2$ (calculated) (T)	138		260							1435	2000
Pocket-H (calculated) (T)	147/165	186	239	368			829				2033

Further, we increased the strength of the magnetic field to explore these weak frequencies. The magnetic torque signals of MoAlB were obtained in magnetic fields up to 59 T below 9.2 K. In our experiment, we used the commercially available silicon piezoresistive microcantilevers fabricated by Seiko Instruments Inc. Cantilever magnetometry is another effective tool to detect a small change in magnetization.[33,34] The sample mounted at the end of a cantilever beam produced magnetic torque $\tau = M \times B$ in a magnetic field, and the resultant small deflection of the beam was detected electrically by measuring the change of the resistance of the cantilever beam.[29] The sensitivity of a cantilever is roughly given by the formula $\frac{\Delta R}{R} = \frac{4\Delta U}{U} = \pi_{\rm L}\frac{6\tau}{(2a)t^2}$,[29] where ΔR is the resistance change, U is the excitation voltage, ΔU is the output voltage from the bridge, $\pi_{\rm L} = 4.5 \times 10^{-10}\,{\rm m^2{\cdot}N^{-1}}$ is the longitudinal piezoresistive coefficient for Si in the [110] direction,[35] and $a = 4\,\mu{\rm m}$ is the leg width. The values correspond to the resistance fluctuation of $\Delta R/R \sim 4.4 \times 10^{-5}$, and the enhanced resolution of the measurement was evaluated as $\tau \sim 3.26 \times 10^{-12}\,{\rm N{\cdot}m}$.

We now focus on the temperature and magnetic field dependences of the oscillating amplitude of magnetic torque with the magnetic field along the b axis. The oscillations torque τ is shown in Fig. 2(g). Figure 2(h) presents the FFT spectrum τ at different temperatures. Three fundamental frequencies can be identified in this figure. The frequency of F_φ is more obvious than those obtained from the Seebeck and Nernst effect measured in the static field. The oscillation frequency is slightly different from thermoelectricity because the sample will be slightly tilted ($\sim$5°) due to the contraction of grease at low temperatures. We fit the temperature dependence of the experimentally observed amplitudes using the Lifshitz–Kosevich (L-K) formula.[36] The oscillation amplitude is proportional to the thermal damping factor $R_{\rm T} = X/\sinh X$, where $X = 14.69m^*T/B$ with m^* being the effective cyclotron mass. We obtained the masses of these frequencies as shown in the inset of Fig. 2(h). The cyclotron mass for different frequencies can be calculated as $m_\alpha = (0.54 \pm 0.02)m_{\rm e}$, $m_\delta = (0.297 \pm 0.007)m_{\rm e}$, and $m_\varphi = (0.33 \pm 0.01)m_{\rm e}$ for the three fundamental frequencies. For metals, the SdH oscillation frequency F is directly related to the orthogonal extremal cross-sectional area ($S_{\rm F}$) as per the Onsager relation $F = (\frac{\hbar}{2e\pi})S_{\rm F}$, $S_{\rm F} = \pi k_{\rm F}^2$, where $k_{\rm F}$ is the Fermi wave-vector, e is the electron charge, and $\hbar$ is the Planck constant. Using the F_φ frequency, we can obtain $k_{\rm F} = 2.53 \times 10^9\,{\rm m^{-1}}$. We take a spherical FS for this frequency at the first approximation to estimate the Fermi energy and carrier density. The Fermi level can be described by $E_{\rm F} = m^* v_{\rm F}^2/2$, where $v_{\rm F}$ is related to $k_{\rm F}$ by $m^* v_{\rm F} = \hbar k_{\rm F}$, $v_{\rm F}$ is the Fermi velocity. This yields a Fermi velocity of $8.89 \times 10^5\,{\rm m/s}$ and a Fermi energy of 0.74 eV. The carrier density is estimated to be $5.5 \times 10^{20}\,{\rm cm^{-3}}$ at the same level as the result from the Hall effect with both carrier densities of $4.2 \times 10^{20}\,{\rm cm^{-3}}$.[20]

We conducted the first-principle calculations to determine the contribution of different pockets for QO. The calculated FS of MoAlB is shown in Fig. 3. The FS comprises two electron pockets ($E1$ and $E2$) and one hole pocket (H). The two electron pockets exhibit 2D anisotropic properties with open orbits. Then, we analyzed the evolution of QO frequencies with the angles and compared them with the experimental results. Figures 4(a) and 4(b) present the angle dependence of frequencies in ab and bc planes, respectively. When $H \| b$, $\theta = 0°$ and $\varphi = 0°$. The circular and square symbols represent the SdH peaks[20] and Seebeck effect, respectively. The lines are obtained from the theoretical result and they are differently colored for each pocket, corresponding to Fig. 3.

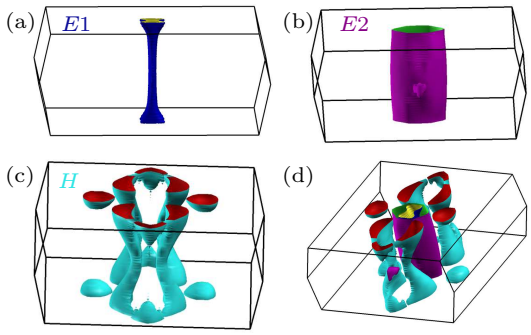

Fig. 3. Calculated Fermi surface of MoAlB. (a) and (b) Electron pockets $E1$ and $E2$. (c) Hole pocket H. (d) Entire Fermi pockets in the Brillouin zone.

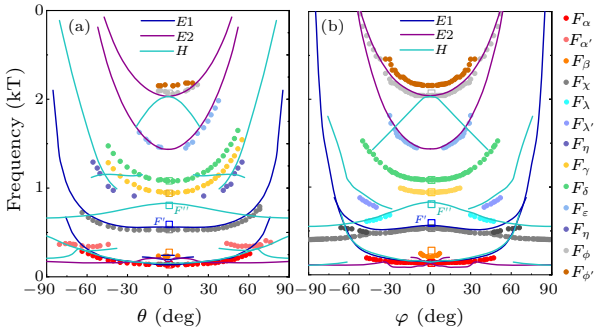

Fig. 4. Angular dependence of the quantum oscillation frequencies extracted from the SdH oscillations (solid circle).[20] The hollow square was extracted from the Seebeck effect in this study and the lines are obtained from the theoretical results.

The angle dependence of the extremal FS cross sections agrees well with the measured SdH frequencies. Our calculated FS indicates that the F_β and F_χ belong to pocket $E1$, F_ε and F_ϕ belong to pocket $E2$,

and F_α, $F_{\alpha'}$, F_λ, and $F_{\lambda'}$ belong to pocket H. Some experimental frequencies were not observed in theoretical calculations, such as F_γ, F_δ, and $F_{\phi'}$. This is probably due to the complex structure of pocket H.

Next, we try to quantitatively evaluate the electrical conductivity anisotropy based on the Boltzmann transport theory using the BoltzTrap2 code and DFT results. BoltzTrap2 adopts a constant relaxation time τ. Although MoAlB is an anisotropic material, τ is proved to be independent of direction to a first approximation in a previous study.[37] We can estimate the anisotropic τ after the calculation. Figure 5 shows the calculated temperature and chemical potential dependences of the electrical conductivity and the electrical conductivity ratios. These ratios ρ_{bb}/ρ_{aa}, ρ_{bb}/ρ_{cc}, and $\rho_{cc}/\rho_{\rm aa}$ are 3.7, 2.4, and 1.6 at 10 K, respectively. As the temperature rises, the ratios slightly increase to 4.9, 3, and 1.8, respectively, at 260 K. However, as the chemical potential is reduced, the three ratios are increased to 9.5, 5, and 2, respectively. The in-plane anisotropy ∼1.5 at low temperatures is comparable to the experimental result of 2.1.

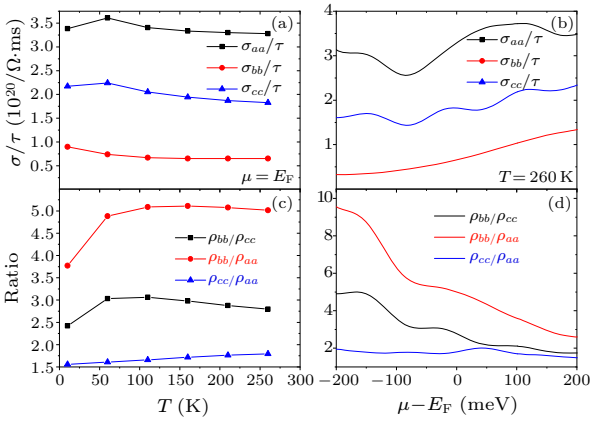

Fig. 5. Calculated diffusive electron conductivity σ over scattering time τ for three orientations in MoAlB. (a) and (b) Temperature dependence of σ/τ and resistivity ratio for three orientations at the Fermi level. (c) and (d) Energy dependence of σ/τ and resistivity ratio for three orientations.

Table 2. Two-dimensional characteristics of MoAlB, and the resistivity anisotropies ($\rho_{\text{out-of-plan}}/\rho_{\text{in-plan}}$) of other layered systems. The fitting coefficients A and B are obtained via $\rho = \rho_0 + AT^2 + BT^5$ and the resistivity values at $\rho_{300\,\rm K}$ and $\rho_{2\,\rm K}$. Notably, b has out-of-plane orientations, instead of the conventional c axis in most materials.

Materials	Ratio at low temperature	Ratio at 300 K
MoAlB (this work)	1126 ($\rho_{bb} = 186.6\,\mu\Omega\cdot$cm/$\rho_{aa} = 0.165\,\mu\Omega\cdot$cm)	177 (ρ_{bb}/ρ_{aa})
	526 ($\rho_{bb} = 186.6\,\mu\Omega\cdot$cm/$\rho_{cc} = 0.35\,\mu\Omega\cdot$cm)	151.6 (ρ_{bb}/ρ_{cc})
	97 ($A_b = 3.64\times10^{-4}\,\mu\Omega$·cm·K^{-2}/$A_a = 3.77\times10^{-6}\,\mu\Omega$·cm·K^{-2})	
	120 ($A_b = 3.64\times10^{-4}\,\mu\Omega$·cm·K^{-2}/$A_c = 3.02\times10^{-6}\,\mu\Omega$·cm·K^{-2})	
	113 ($B_b = 6.16\times10^{-7}\,\mu\Omega$·cm·K^{-5}/$B_a = 5.43\times10^{-9}\,\mu\Omega$·cm·K^{-5})	
	224 ($B_b = 6.16\times10^{-7}\,\mu\Omega$·cm·K^{-5}/$B_c = 2.75\times10^{-9}\,\mu\Omega$·cm·K^{-5})	
Sr_2RuO_4[38]	∼500 (4–80 K)	30
MoAlB[19]	1.43×10^5 (ρ_{bb}/ρ_{aa}) (2 K)	6.8×10^3 (ρ_{bb}/ρ_{aa})
	1.1×10^4 (ρ_{bb}/ρ_{cc}) (2 K)	3.9×10^3 (ρ_{bb}/ρ_{cc})
Graphite[39,40]	500	
WTe_2[41]	14.4 (obtained by μ_b/μ_c)	
$PdCoO_2$[42]	1000 ($\rho_c/\rho_{\rm ab}$) (2 K)	250
YBCO ($T_c = 92.5K$)[43]	96 (100 K)	
La_2CuO_4 based systems[44]	40–170 (obtained by $H_{c2\parallel}/H_{c2\perp}$)	
Bi2212 (T_c = 76–89)[45]	(4–14) ×10^4 (∼80 K) (ρ_c is semiconductor-like)	(5–9) ×10^4
Fe(Se,Te)[46]	10–27 (10 K)	3–18
$CsCa_2Fe_4As_4F_2$[47]	3150 (30 K, partially semiconductor-like along ρ_c)	730
$BaFe_2As_2$[48]	∼150	∼150
ZrSiSe[49]	∼4.3 (∼4 K)	∼3.4
ZrSiS[50]	∼5 (∼4 K)	∼8
ReS_2[50]	$\sim2\times10^5$ (∼70 K, semiconductor)	$\sim5\times10^5$
$ReSe_2$[50]	∼300 (∼90 K, semiconductor)	$\sim6\times10^5$
WS_2[51]	194 (208 K, semiconductor)	8
MoS_2[51]	∼2000 (90 K, semiconductor)	100

Surprisingly, the anisotropy of the out-of-plane electrical conductivity differs considerably from the experimental results at low temperatures. The calculated ρ_{bb}/ρ_{aa} and ρ_{bb}/ρ_{cc} are only around 3, compared to $\rho_{bb}/\rho_{aa} = 1126$ and $\rho_{bb}/\rho_{cc} = 526$ obtained from the experiment. The temperature dependence of ρ_{bb}/ρ_{cc} is nearly constant, while it is enhanced by two orders experimentally. Thus, the isotropic τ approximation is invalid and τ is quite anisotropic in the present case. Using the carrier density $p = n = 2.1\times10^{20}\,\rm cm^{-3}$,[20] we can estimate the mean free path (MFP) from the resistivity $\ell = \frac{\hbar\sqrt[3]{3\pi^2 n}}{e^2 n\rho}$. The MFPs ℓ_{aa}, ℓ_{bb}, and ℓ_{cc} are 13.7 μm, 12.2 nm, and 6.5 μm based on the resistivities of 0.165,

186.6, and 0.35 μΩ·cm, respectively. Notably, the lattice constants are $a = 3.2162$ Å, $b = 14.062$ Å, and $c = 3.1030$ Å.[20] The MFP ℓ_{bb} along the b axis is only 8.7 times larger than the lattice constant, approaching the Mott–Ioffe–Regel limit ($\ell_{bb} \approx b$). At low temperatures, the semiconductor behavior with a slight increase in the temperature dependence of the resistivity (shown in the inset of Fig. 1) may be attributed to the Kondo effect due to a small amount of molybdenum severing as the impurity scattering center or due to incoherent hopping, which is found in several layered materials.[52–54] In a previous report,[19] ρ_{bb} is 46.9 mΩ·cm at 2 K and 121.8 mΩ·cm at 300 K. These values seem too large. Here, ℓ_{bb} can be estimated to be 2.25×10^{-12} m and 8.66×10^{-12} m, which are two orders smaller than the lattice constant along the b axis. This would result in an insulting behavior of the temperature dependent resistivity ρ_{bb}, in contrast to the experimental results. Compared with the theoretical FS, the main anisotropic electronic properties would result from electron-like bands.

Further, we compared the out-of-plane anisotropy of MoAlB with those of some typical anisotropic materials, including graphite, cuprates, iron-based superconductors, and transition metal dichalcogenides. Table 2 lists the electrical conductivity ratios of these materials. The anisotropic ratio of 1100 is comparable to the layered metals $PdCoO_2$, which is nonmagnetic with a similar interlayer MFP/lattice of 11. The anisotropic ratio is larger than those of typical anisotropic semimetals WTe_2, Fe(Se,Te), ZrSiSe, ZrSiS, and some semiconductors, such as WS_2. The anisotropic ratio in some semiconductors such as ReS_2, $ReSe_2$, and MoS_2 can reach beyond 10^5. The cuprate Bi2212 reaches 10^5, hosting an in-plane metallic behavior and an out-of-plane insulating behavior. Thus, the anisotropy of 526 in the semimetal MoAlB implies a large anisotropy among these anisotropic layered semimetals, comparable to graphite and Sr_2RuO_4. This anisotropy would be mainly due to the anisotropic electron–electron scattering. Moreover, the ratios of $A_b/A_{a,c}$ and $B_b/B_{a,c}$ are large. In Sr_2RuO_4, $\rho = \rho_0 + AT^2$ can describe the temperature dependence of resistivity for both orientations, dominated by the umklapp process of e–e scattering.

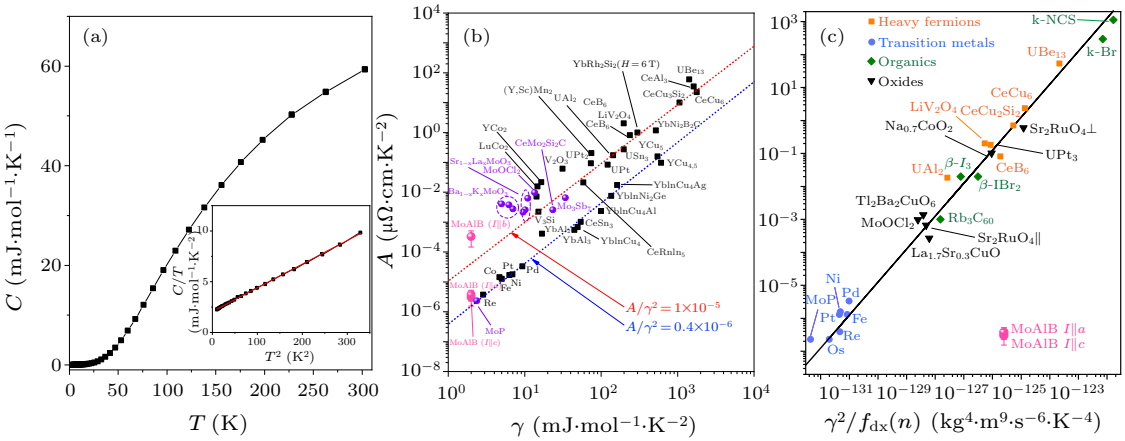

Fig. 6. (a) Temperature dependence of the zero-field specific heat of MoAlB from 3 to 300 K. The inset shows C/T as a function of T^2. (b) Kadowaki–Woods plot of MoAlB. The Red and blue lines represent the universal lines for heavy-fermion compounds and ordinary transition metals, respectively. MoAlB data are shown by the pink spheres, and other molybdenum compounds are shown using the purple spheres. (c) The modified Kadowaki–Woods ratio of our MoAlB in the basal plane (pink spheres). Other data of strong electron–electron correlated materials are taken from Refs. [25,55,56].

To further understand the electronic properties of the hard material MoAlB, we performed specific heat measurements to determine its electronic specific heat γ. Figure 6(a) presents the temperature dependence of the zero-field specific heat C, from 3 K to 300 K. The inset of Fig. 6(a) shows the fitting of the equation $C/T = \gamma + \beta T^2$, where γ is the electron term and β represents the phonon contribution. Our results $\gamma = 2$ mJ·mol^{-1}·K^{-2} and $\beta = 2.33 \times 10^{-5}$ mJ·mol^{-1}·K^{-4} are close to the results obtained using polycrystals.[15,57] Following the free-electron model, γ can be related to the density of electronic states at the Fermi level $N(E_F) = \frac{3\gamma}{\pi^2 k_B^2}$ and $N(E_F)$ was obtained to be 3.39 states/(eV·u.c.) with u.c. denoting unit cell, which is also comparable to the value 3.2 states/(eV·u.c.) calculated from the first principles.[58] Therefore, the Fermi energy $\varepsilon_F = 0.71$ eV can be inferred by considering the volume of a unit cell, which is thus close to the experimental result obtained from the QO of F_φ. This is understandable because the largest electronic pocket would contribute more to the physical properties. The

Debye temperature can also be inferred from $\theta_{\rm D} = (12\pi^4 RZ/5\beta)^{1/3}$, where $R = 8.314\,{\rm J\cdot mol^{-1}\cdot K^{-1}}$ is the molar gas constant and Z is the number of atoms in a unit cell (Fig. 1). The obtained high Debye temperature $\theta_{\rm D} = 693\,{\rm K}$ is consistent with the interesting characteristics of its high melting point and hardness.

Once the KWR is obtained using γ, we can verify the Fermi liquid behavior in this hard material and its accordance with other transition metals. A in Eq. (1) is known to be one of the intrinsic properties of metals, and it is squarely proportional to quasiparticle mass enhancement due to strong electron correlation.[59,60] Because the FS exhibits obvious 2D anisotropic properties, we calculated the in-plane and out-of-plane KWRs [Fig. 6(b)]. The KWR also shows a large anisotropy. In the plane, the values of $\alpha_a = 0.943 \times 10^{-6}\,{\rm \mu\Omega\cdot cm\cdot mol^2\cdot K^2\cdot mJ^{-2}}$ and $\alpha_c = 0.755 \times 10^{-6}\,{\rm \mu\Omega\cdot cm\cdot mol^2\cdot K^2\cdot mJ^{-2}}$ are close to those in the ordinary transition metals $\alpha_{\rm TM}$. However, the out-of-plane $\alpha_b = 9.1\times10^{-5}\,{\rm \mu\Omega\cdot cm\cdot mol^2\cdot K^2\cdot mJ^{-2}}$ is considerably larger and closer to the $\alpha_{\rm HF}$ value for heavy-fermion compounds. Such a highly different ratio of A/γ^2 matches the quasi-2D FS structure, indicating that similar quasiparticles have small interlayer dispersion. This phenomenon resembles the case of Sr_2RuO_4, where the in-plane $A_{\rm ab}/\gamma^2$ is consistent with the universal trend and the out-of-plane A_c/γ^2 dramatically deviates from the universality. The anisotropy of KWR is ascribed to the dimensionality, which would be of the same reason for MoAlB.

It is instructive to compare the KWR of MoAlB with other molybdenum compounds, except nonmagnetic MoP, which normally exhibits large KWRs. Figure 6(b) includes the KWRs of other molybdenum compounds Mo_3Sb_7, $MoOCl_2$, $Sr_{1-x}La_xMoO_3$, and $Ba_{1-x}K_xMoO_3$ from previous studies.[24–27] The enhanced KWR was attributed to the spin fluctuation scenario in Mo_3Sb_7.[24,61] In the triple point topological metal MoP, another nonmagnetic molybdenum, the KWR is close to the value for the in-plane KWR of MoAlB.

Although the KWRs for the in-plane and out-of-plane Sr_2RuO_4 are different, a modified form was proposed to unify the discrepancy and difference of material types.[55] The modified form is expressed as $\tilde{\alpha} = \frac{Af_{\rm dx}(n)}{\gamma^2} = \frac{81}{4\pi\hbar k_{\rm B}^2 e^2} = 1.25 \times 10^{118}\,{\rm \Omega\cdot kg^{-4}\cdot m^{-8}\cdot s^6\cdot K^2}$, where $f_{\rm dx}(n)$ is a material-dependent factor. For the in-plane transport, we have $f_2(n) = \frac{n^2}{\pi\hbar^2 l}$, where l is the interlayer spacing, rendering a modified KWR of $\tilde{\alpha_a} = 1.49 \times 10^{112}\,{\rm \Omega\cdot kg^{-4}\cdot m^{-8}\cdot s^6\cdot K^2}$ and $\tilde{\alpha_c} = 1.19\times10^{112}\,{\rm \Omega\cdot kg^{-4}\cdot m^{-8}\cdot s^6\cdot K^2}$. After summarizing the results in Fig. 6(c), two outstanding features emerge in MoAlB. First, the unified KWR in the MoP is consistent with the theory and the in-plane-modified KWR of MoAlB dramatically deviated from the unified line. Notably, we cannot obtain the modified out-of-plane KWR because the interlayer hopping integral is unknown at this stage. MoAlB and MoP have similar values of A, γ, and A/γ^2. However, one difference is that the carrier density of MoAlB is two orders smaller than that of MoP.[56] Second, the anisotropy of KWR is comparable in the layered MoAlB and Sr_2RuO_4 because of their two-dimensionality in the two systems, leading to a 2D Fermi liquid behavior. The in-plane $A_{a,c}/\gamma^2$ for MoAlB agrees with the universal trend, but the out-of-plane A_b/γ^2 severely deviates from the universality. This indicates that the quasiparticles essentially form a 2D Fermi liquid and A_b reflects a small interlayer dispersion of the same quasiparticles.[38] However, both unified KWRs in-plane and out-of-plane in Sr_2RuO_4 can be rescaled and the in-plane modified KWR of MoAlB cannot be rescaled into the theoretical line. Notably, they have a similar anisotropic value ∼500. The difference is that the carrier density of MoAlB is two orders lower than $5.4 \times 10^{22}\,{\rm cm^{-3}}$ of Sr_2RuO_4.[62] The unexceptional anisotropic Fermi liquid properties would render MoAlB as a unique platform to study the KWR.

In conclusion, we have explored the properties of the FS of the layered ternary boride MoAlB by combining the first-principles calculations and QOs with various techniques. There is a good agreement between the theoretical calculations and the experiment results, indicating that the FS comprises two sheets of anisotropic electron pockets and one complex sheet of hole pocket. In addition, we observe that MoAlB has a large out-of-plane electrical anisotropy ($\rho_{bb}/\rho_{aa} \sim 1100$). For the in-plane KWR, $A_{a,c}/\gamma^2$ is closer to the behavior of ordinary transition metals, but for the out-of-plane KWR, A_b/γ^2 is considerably larger and highly deviated from the universality. Unlike other layered systems (Sr_2RuO_4 and $MoOCl_2$), the in-plane KWR of MoAlB cannot be unified using the modified KWR formula. The present findings may provide a helpful basis for exploring 2D Fermi liquid behavior of layered molybdenum compounds.

Acknowledgments. This work was supported by the National Natural Science Foundation of China (Grant Nos. 12004123, 51861135104, and 11574097), the National Key Research and Development Program of China (Grant No. 2016YFA0401704), the Fundamental Research Funds for the Central Universities (Grant No. 2019kfyXMBZ071), and the China Postdoctoral Science Foundation (Grant No. 2018M630846).

References

[1] Kota S, Sokol M and Barsoum M W 2020 *Int. Mater. Rev.* **65** 226
[2] Lu J, Kota S, Barsoum M W and Hultman L 2017 *Mater.*

Res. Lett. **5** 235
[3] Gong Y, Guo B, Wang X, Ye W, Li R, Chen X, Wang J and Zhang G 2020 *Int. J. Refract. Met. Hard Mater.* **93** 105345
[4] Ade M and Hillebrecht H 2015 *Inorg. Chem.* **54** 6122
[5] Qi X X, Song G P, Yin W L, Wang M F, He X D, Zheng Y T, Wang R G and Bai Y L 2020 *J. Inorg. Mater.* **35** 53
[6] Bai Y, Qi X, He X, Sun D, Kong F, Zheng Y, Wang R and Duff A I 2019 *J. Am. Ceram. Soc.* **102** 3715
[7] Jeitschko W 1969 *Acta Crystallogr. Sect. B* **25** 163
[8] Becher H J, Krogmann K and Peisker E 1966 *Z. Anorg. Allg. Chem.* **344** 140
[9] Jeitschko W 1966 *Monatshefte Chemie* **97** 1472
[10] Xiang H, Feng Z, Li Z and Zhou Y 2018 *J. Alloys Compd.* **738** 461
[11] Jung W and Petry K 1988 *Z. Kristallographie* **182** 153
[12] Su X, Dong J, Chu L, Sun H, Grasso S and Hu C 2020 *Ceram. Int.* **46** 15214
[13] Kota S, Zapata-Solvas E, Ly A, Lu J, Elkassabany O, Huon A, Lee W E, Hultman L, May S J and Barsoum M W 2016 *Sci. Rep.* **6** 1
[14] Lu X, Li S, Zhang W, Yu W and Zhou Y 2019 *Ceram. Int.* **45** 9386
[15] Kota S, Agne M, Zapata-Solvas E, Dezellus O, Lopez D, Gardiola B, Radovic M and Barsoum M W 2017 *Phys. Rev. B* **95** 144108
[16] Alameda L T, Moradifar P, Metzger Z P, Alem N and Schaak R E 2018 *J. Am. Chem. Soc.* **140** 8833
[17] Alameda L T, Holder C F, Fenton J L and Schaak R E 2017 *Chem. Mater.* **29** 8953
[18] Akopov G, Yeung M T and Kaner R B 2017 *Adv. Mater.* **29** 1604506
[19] Huang Y, Si J, Lin S, Lv H, Song W, Zhang R, Luo X, Lu W, Zhu X and Sun Y 2022 *Small* **18** 2104460
[20] Zhao L, Xu L, Ding L, Zuo H and Zhu Z 2020 *Phys. Rev. B* **102** 075139
[21] Miyake K, Matsuura T and Varma C M 1989 *Solid State Commun.* **71** 1149
[22] Rice M J 1968 *Phys. Rev. Lett.* **20** 1439
[23] Kadowaki K and Woods S 1986 *Solid State Commun.* **58** 507
[24] Candolfi C, Lenoir B, Dauscher A, Bellouard C, Hejtmánek J, Šantavá E and Tobola J 2007 *Phys. Rev. Lett.* **99** 037006
[25] Wang Z, Huang M, Zhao J, Chen C, Huang H, Wang X, Liu P, Wang J, Xiang J, Feng C, Zhang Z, Cui X, Lu Y, Yang S A and Xiang B 2020 *Phys. Rev. Mater.* **4** 041001
[26] Zhang S B, Sun Y P, Zhao B C, Ang R, Zhu X B and Song W H 2009 *J. Alloys Compd.* **479** 22
[27] Zhang S B, Sun Y P, Zhao B C, Zhu X B and Song W H 2006 *Phys. Status Solidi B* **243** 1331
[28] Wang J, Nie P, Li X, Zuo H, Fauqué B, Zhu Z and Behnia K 2020 *Proc. Natl. Acad. Sci. USA* **117** 30215
[29] Ohmichi E and Osada T 2002 *Rev. Sci. Instrum.* **73** 3022
[30] Blaha P, Schwarz K, Tran F, Laskowski R, Madsen G K H and Marks L D 2020 *J. Chem. Phys.* **152** 074101
[31] Madsen G K H, Carrete J and Verstraete M J 2018 *Comput. Phys. Commun.* **231** 140
[32] Ziman J M 1972 *Principles of the Theory of Solids* (Cambridge: Cambridge University Press)
[33] Naughton M J, Ulmet J P, Narjis A, Askenazy S, Chaparala M V and Hope A P 1997 *Rev. Sci. Instrum.* **68** 4061
[34] Naughton M J, Ulmet J P, Narjis A, Askenazy S, Chaparala M V and Richter R 1998 *Physica B* **246-247** 125
[35] Kanda Y 1991 *Sens. Actuators A* **28** 83
[36] Lifshitz I and Kosevich A 1956 *Sov. Phys. JETP* **2** 636
[37] Madsena G K H and Singhb D J 2006 *Comput. Phys. Commun.* **175** 67
[38] Maeno Y, Yoshida K, Hashimoto H, Nishizaki S, Ikeda S I, Nohara M, Fujita T, Mackenzie A P, Hussey N E, Bednorz J G and Lichtenberg F 1997 *J. Phys. Soc. Jpn.* **66** 1405
[39] Zhu Z, Nie P, Fauqué B, Vignolle B, Proust C, McDonald R D, Harrison N and Behnia K 2019 *Phys. Rev. X* **9** 011058
[40] Primak W and Fuchs L H 1954 *Phys. Rev.* **95** 22
[41] Zhu Z, Lin X, Liu J, Fauqué B, Tao Q, Yang C, Shi Y and Behnia K 2015 *Phys. Rev. Lett.* **114** 176601
[42] Hicks C W, Gibbs A S, Mackenzie A P, Takatsu H, Maeno Y and Yelland E A 2012 *Phys. Rev. Lett.* **109** 116401
[43] Holm W, Andersson M, Rapp Ö, Kulikov M A and Makarenko I N 1993 *Phys. Rev. B* **48** 4227
[44] Shamoto S, Onoda M, Sato M and Hosoya S 1987 *Solid State Commun.* **62** 479
[45] Chen X H, Yu M, Ruan K Q, Li S Y, Gui Z, Zhang G C and Cao L Z 1998 *Phys. Rev. B* **58** 14219
[46] Bryja H, Hühne R, Iida K, Molatta S, Sala A, Putti M, Schultz L, Nielsch K and Hänisch J 2017 *Supercond. Sci. Technol.* **30** 115008
[47] Wang Z C, Liu Y, Wu S Q, Shao Y T, Ren Z and Cao G H 2019 *Phys. Rev. B* **99** 144501
[48] Wang X F, Wu T, Wu G, Chen H, Xie Y L, Ying J J, Yan Y J, Liu R H and Chen X H 2009 *Phys. Rev. Lett.* **102** 117005
[49] Shirer K R, Modic K A, Zimmerling T, Bachmann M D, König M, Moll P J W, Schoop L and Mackenzie A P 2019 *APL Mater.* **7** 101116
[50] Tiong K K, Ho C H and Huang Y S 1999 *Solid State Commun.* **111** 635
[51] Pisoni A, Jacimovic J, Gaál R, Náfrádi B, Berger H, Révay Z and Forró L 2016 *Scr. Mater.* **114** 48
[52] Zhang C, Chen X, Almasan C, Gardner J and Sarrao J 2002 *Phys. Rev. B* **65** 134439
[53] Limelette P, Hardy V, Auban-Senzier P, Jérome D, Flahaut D, Hébert S, Frésard R, Simon C, Noudem J and Maignan A 2005 *Phys. Rev. B* **71** 233108
[54] Salvetat J P, Berger H, Halbritter A, Mihaly G, Pavuna D and Forro L 2000 *Europhys. Lett.* **52** 584
[55] Jacko A, Fjærestad J and Powell B 2009 *Nat. Phys.* **5** 422
[56] Kumar N, Sun Y, Nicklas M, Watzman S J, Young O, Leermakers I, Hornung J, Klotz J, Gooth J, Manna K *et al.* 2019 *Nat. Commun.* **10** 1
[57] Bai Y, Qi X, Duff A, Li N, Kong F, He X, Wang R and Lee W E 2017 *Acta Mater.* **132** 69
[58] Gunst T, Markussen T, Stokbro K and Brandbyge M 2016 *Phys. Rev. B* **93** 035414
[59] Lin X, Fauqué B and Behnia K 2015 *Science* **349** 945
[60] Wang J, Wu J, Wang T, Xu Z, Wu J, Hu W, Ren Z, Liu S, Behnia K and Lin X 2020 *Nat. Commun.* **11** 1
[61] Koyama T, Yamashita H, Takahashi Y, Kohara T, Watanabe I, Tabata Y and Nakamura H 2008 *Phys. Rev. Lett.* **101** 126404
[62] Mackenzie A P, Hussey N E, Diver A J, Julian S R, Maeno Y, Nishizaki S and Fujita T 1996 *Phys. Rev. B* **54** 7425